Atmos. Chem. Phys. Discuss., 13, 24925–24973, 2013
www.atmos-chem-phys-discuss.net/13/24925/2013/
doi:10.5194/acpd-13-24925-2013

Atmospheric Chemistry and Physics Discussions

Impacts of different plant functional types on ambient ozone predictions in the Seoul Metropolitan Areas (SMA), Korea

H.-K. Kim[1], J.-H. Woo[1], R. S. Park[2], C. H. Song[2], J.-H. Kim[3], S.-J. Ban[4], and J.-H. Park[4]

[1]Department of Advanced Technology Fusion, Konkuk University, Seoul, Korea
[2]School of Environmental Science and Engineering, Gwangju Institute of Science and Technology, Gwangju, Korea
[3]Green-ECOS, Seoul, Korea
[4]Air Quality Research Division, National Institute of Environmental Research, Incheon, Korea

Received: 8 July 2013 – Accepted: 10 September 2013 – Published: 25 September 2013

Correspondence to: J.-H. Woo (jwoo@konkuk.ac.kr)

Published by Copernicus Publications on behalf of the European Geosciences Union.

Abstract

Plant functional type (PFT) distributions affect the results of biogenic emission modeling as well as O_3 and PM simulations using chemistry-transport models (CTMs). This paper analyzes the variations of both surface biogenic VOC emissions and O_3 concentrations due to changes in the PFT distributions in the Seoul Metropolitan Areas, Korea. Also, this paper attempts to provide important implications for biogenic emissions modeling studies for CTM simulations. MM5-MEGAN-SMOKE-CMAQ model simulations were implemented over the Seoul Metropolitan Areas in Korea to predict surface O_3 concentrations for the period of 1 May to 31 June 2008. Starting from MEGAN biogenic emissions analysis with three different sources of PFT input data, US EPA CMAQ O_3 simulation results were evaluated by surface O_3 monitoring datasets and further considered on the basis of geospatial and statistical analyses. The three PFT datasets considered were "(1)KORPFT", developed with a region specific vegetation database; (2) CDP, adopted from US NCAR; and (3) MODIS, reclassified from the NASA Terra and Aqua combined land cover products. Comparisons of MEGAN biogenic emission results with the three different PFT data showed that broadleaf trees (BT) are the most significant contributor, followed by needleleaf trees (NT), shrub (SB), and herbaceous plants (HB) to the total biogenic volatile organic compounds (BVOCs). In addition, isoprene from BT and terpene from NT were recognized as significant primary and secondary BVOC species in terms of BVOC emissions distributions and O_3-forming potentials in the study domain. Multiple regression analyses with the different PFT data (δO_3 vs. δPFTs) suggest that KORPFT can provide reasonable information to the framework of MEGAN biogenic emissions modeling and CTM O_3 predictions. Analyses of the CMAQ performance statistics suggest that deviations of BT areas can significantly affect CMAQ isoprene and O_3 predictions. From further evaluations of the isoprene and O_3 prediction results, we explored the PFT area-loss artifact that occurs due to geographical disparity between the PFT and leaf area index distributions, and can cause increased bias in CMAQ O_3. Thus, the PFT-loss artifact must be a source

ACPD
13, 24925–24973, 2013

of limitation in the MEGAN biogenic emission modeling and the CTM O_3 simulation results. Time changes of CMAQ O_3 distributions with the different PFT scenarios suggest that hourly and local impacts from the different PFT distributions on occasional interdeviations of O_3 are quite noticeable, reaching up to 10 ppb. Exponentially diverging hourly BVOC emissions and O_3 concentrations with increasing ambient temperature suggest that the use of representative PFT distributions becomes more critical for O_3 air quality modeling (or forecasting) in support of air quality decision-making and human health studies.

1 Introduction

Biogenic volatile organic compounds (BVOCs) emitted from vegetated areas play an important role in the chemistry of the lower troposphere and atmospheric boundary layer via a series of oxidation reactions with the OH and NO_3 radicals and O_3 (Finlayson-Pitts and Fitts, 2000; Atkinson and Arey, 2003). It has been known that BVOC emissions can enhance O_3 formation in the areas with high NO_x concentrations, because the BVOC oxidation increases the concentrations of hydroperoxy and organic peroxy radicals (HO_2 and RO_2) that can convert NO into NO_2 without depleting O_3. In addition, the BVOC emissions can reduce O_3 concentrations in the areas with low levels of NO_x, because the reaction of O_3 and BVOC reduces hydroxyl radicals and leads to decreased O_3 formation (Finlayson-Pitts and Fitts, 2000; Hogrefe et al., 2011). For example, a regional air-quality modeling study reported that biogenic emissions are associated with at least 20 % of surface O_3 concentrations in most areas of the continental United States (Tao et al., 2003). A global chemistry transport modeling with MOZART-4 (Model for Ozone and Related Chemical Species, version 4) reported that biogenic isoprene emissions cause −5 ppb to 10 ppb changes in surface O_3 concentrations over the Amazon region, Indonesia, and parts of South Africa during the spring season (Pfister et al., 2008).

ACPD
13, 24925–24973, 2013

The flux of biogenic emission is a strong function of vegetation area, biomass density, and other environmental factors (Guenther et al., 1995, 2006). In biogenic emission modeling, vegetation area has been commonly considered to be one of the most important driving variables because it reflects the phenological emission capacity of the area of interest. In order to more efficiently prepare vegetation area information as an input to biogenic emission modeling, plant functional type (PFT) data have been used (Guenther et al., 2006; Pfister et al., 2008; Arneth et al., 2011). Conceptually, PFTs are classes of vegetation species that share similar responses to environmental factors, similar functioning at the organismic level, and/or similar effects on ecosystems (Smith et al., 1997; Sun et al., 2008). In a biogenic emissions modeling approach, the PFT datasets specify the type and composition of vegetation classes in a grid cell to determine the capacity of biogenic emissions. Thus, careful consideration of PFT distributions is needed for the estimation of biogenic emissions and subsequent predictive works such as the O_3 prediction with CTM.

Several recent modeling studies have reported sensitivities of PFT to the biogenic emissions and O_3 concentrations. For example, Guenther et al. (2006) reported about −13 to 24 % changes in global annual isoprene emissions from standard Model of Emissions of Gases and Aerosols from Nature (MEGAN) modeling using the 11 different PFT datasets. Pfister et al. (2008) reported a factor of two or more differences in monthly isoprene emissions on global to regional scales through the examination of the MEGAN sensitivity to three different sets of satellite-derived leaf area index (LAI) and PFT datasets. Pfister et al. (2008) also reported an inter-difference of up to 5 ppb in monthly mean O_3 concentrations from the global scale simulations of MOZART /MEGAN with three different sets of satellite-derived LAI and PFT input data.

Although the previously summarized modeling studies produced valuable findings, none of the studies represents a local scale and a more detailed situation. For example, Pfister et al. (2008) adopted a coarse grid resolution (i.e., $2.8^{\circ} \times 2.8^{\circ}$) in their study and use only satellite-based PFT distributions for their global modeling study to carry out. In addition, they also showed that the sensitivity or uncertainty (e.g., a factor of 2 or

ACPD
13, 24925–24973, 2013

more differences in isoprene and up to 5 ppb of surface O_3 inter-deviation) is not only related to changes in LAI data but also changes in PFT data.

The purpose of our study is to investigate the impacts of different PFT distribution data on O_3 concentrations. Carrying out biogenic emission model and CTM simulations, we investigated changes in surface biogenic emissions and ambient O_3 concentrations with different PFT distribution datasets. Our approach has several distinctive features. First, in this study, we included a region-specific high-resolution PFT distribution dataset: the Korean PFT database (KORPFT). The KORPFT was derived from 3 datasets: (1) Korean land cover classification maps; (2) tree stock maps; and (3) Korean vegetation survey data. Secondly, we adopted a 3 km by 3 km fine grid system in order to more closely investigate spatial patterns of biogenic emissions and O_3 behaviour in accordance with more fine PFT distribution patterns. Thirdly, we changed only PFT datasets without changing any other model input configurations, such as LAI, meteorological or chemical variables, in order to isolate the impacts of the different PFTs on atmospheric chemistry (or O_3 concentrations).

The main idea behind our approach is that because PFT distributions affect the magnitudes of biogenic emission capacity in the domain of interest, the use of different PFT data can affect biogenic emission estimations and consequently O_3 prediction performances. The proposed idea and method was tested over the Seoul Metropolitan Areas (SMA) in Korea, in which both tremendously developed urban area and densely vegetated areas actually coexist. Recently, the Korean Ministry of Environment (MoE) promulgated the Special Act on Metropolitan Air Quality Improvement (SAMAQI) Phase-II that will be enforced in 2015 (Ministry of Environment, 2012a). To support air quality control activities associated with SAMAQI Phase-II, the MoE has decided to execute over 4.7 trillion Korean Won (4.11 billion USD) for the fiscal period of 2015–2024 (KEI and KOSAE, 2012). Originally, the SAMAQI Phase-I was enacted in December 2003 and enforced in January 2005 with an aim to attain the air quality levels for SO_2, CO, NO_2 and PM_{10} in the SMA comparable to those in the major cities of the developed countries (Tokyo, New York, Paris, etc.). Through the SAMAQI Phase-I involving

ACPD
13, 24925–24973, 2013

a number of and high cost of air quality control activities, the SMA has achieved the remarkable improvement in SO_2 and CO air quality but not in PM_{10} and NO_2 air quality (Ministry of Environment, 2012b). The SAMAQI Phase-II places considerable emphasis on $PM_{2.5}$, NO_2, VOC and O_3 pollutions that underscore the priority on improving the quality of human life and protecting human health from air pollution. Under the SAMAQI Phase-II, the SMA municipal government has to establish the implementation plans (IPs) for air quality attainment for those pollutants across the SMA (Ministry of Environment, 2012a). In these circumstances, biogenic source emissions are considered as one of the basis for IP planning and modeling inventories to manage O_3 and $PM_{2.5}$ air quality in the SMA. Moreover, it is commonly accepted that there are big uncertainties for characterizing biogenic emission sources and determining emission amounts although many efforts to improve emission inventory have been made in the past decade in Korea. The findings presented in this study can provide important implications to air quality supporting groups of the municipal governments for designing and implementing biogenic emission estimation strategies in the SMA.

Section 2 of this manuscript describes the PFT distribution datasets developed for or used in this study together with the simulation framework used for biogenic emission estimation and O_3 predictions and some statistical measures used for the evaluation of the modeling results. Sect. 3 presents and discusses comparison and evaluation results for biogenic emissions and O_3. Finally, Sect. 4 presents some conclusions for this study.

ACPD
13, 24925–24973, 2013

2 PFT datasets and simulation experiment

2.1 Development of the PFT dataset

2.1.1 Korean PFT database

A high-resolved PFT distribution dataset (resolution of $150 \times 150\,m^2$) for the Korean Peninsula was established in this study (hereafter KORPFT) by compiling various local sources of vegetation data, such as Korean land cover map (produced in 2007 and renewed in 2009) and vegetation survey (collected for the consecutive years 1994–2004) from the Korea Ministry of Environment, and tree stock maps (produced and renewed for the consecutive years 1996–2005) from the Korea Forest Service.

A four-PFT scheme in which multiple vegetation species were classified into four types, broadleaf (BT), needleleaf (NT), shrub (SB), and herbaceous (HB), was applied. The fraction of individual PFT groups ($PFTF_k$) was calculated by applying the canopy density weighted focal average as follows:

$$PFTF_k\,(\%) = \sum_{i=1}^{n} fm_{PFT_{k\_i}}/SA \;\times \delta_{PFT_{k\_i}} \times 100 \qquad (1)$$

where SA is a selected grid region (m^2) with n-grid cells; $PFTF_k$ denotes the percent area of an individual PFT in the SA (%); k denotes the individual PFT type (e.g., BT, NT, SB, and HB); n denotes the number of unit grid cells in the SA; $fm_{PFT_{k\_i}}$ is the spatial moving averaged value (m^2) of the i-th unit grid cell for a PFT in the SA calculated by the focal average method; and $\delta_{PFT_{k\_i}}$ is the vegetation canopy density factor for an individual PFT at i-th grid cell ($0 \le \delta_{PFT_{k\_i}} \le 1$).

ACPD
13, 24925–24973, 2013

The focal average of individual PFTs at every focal grid cell (the *i*-th grid cell) can be defined as follows:

$$\mathrm{fm}_{\mathrm{PFT}_{k\_i}} = \frac{1}{N_i} \sum_{\{j:j\sim i\}}^{n} a_{j_{\mathrm{wrt}}\mathrm{PFT}_k}, \quad (2)$$

where N_i denotes the number of all neighbors of the *i*-th unit grid cell, the set $\{j : j \sim i\}$ contains all the neighboring locations *j* of unit *i*, and $a_{j_{\mathrm{wrt}}\mathrm{PFT}_k}$ is the area sum (m^2) of all neighboring grids of a focal grid cell with respect to an individual PFT group.

2.1.2 CDP and MODIS PFT

Two other PFT distribution datasets used in this study are based on satellite observations. The former PFT distribution dataset (resolution of $1 \times 1\,\mathrm{km}^2$) was developed for the global isoprene emission study (Guenther et al., 2006) and derived from Moderate Resolution Imaging Spectroradiometer (MODIS) land cover product in 2001. As this PFT dataset is downloadable from the community data portal (URL: http://cdp.ucar.edu) maintained by US National Center for Atmospheric Research (NCAR), we refer to this dataset as CDP for brevity in this study. The latter PFT distribution dataset (resolution of $0.5 \times 0.5\,\mathrm{km}^2$) was reclassified for this study from the MODIS land cover type 5 products of the Terra and Aqua satellite sensors in 2008 (hereafter MODIS). The MODIS land cover type 5 data, with a PFT scheme including eight vegetation and four non-vegetation classes (Bonan et al., 2002; Friedl et al., 2002; Strahler et al., 1999), were processed to generate the MEGAN PFT. The MODIS vegetation classes were converted into MEGAN PFT classes by straightforward mapping of the eight MODIS vegetation classes into the four MEGAN PFTs (i.e., BT, NT, SB, and HB). For example, the PFT distribution was calculated by adopting land-cover class descriptions provided by the International Geosphere-Biosphere Programme (IGBP) (Friedl et al., 2002; Strahler et al., 1999). As an example, the MEGAN BT was calculated by 80 % × [broadleaf evergreen trees + broadleaf deciduous trees].

ACPD
13, 24925–24973, 2013

2.2 Framework of the simulation experiment

A modeling framework, the Fifth-Generation NCAR/Pennsylvania State Meso-scale Model (MM5)/the Sparse Matrix Operator Kernel Emissions (SMOKE)/the Model of Emissions of Gases and Aerosols from Nature (MEGAN)/the Community Multiscale Air Quality (CMAQ) was established for meteorological modeling, anthropogenic and biogenic emissions processing and modeling, and chemistry-transport model simulations for May–June 2008. In this modeling study, 3-step nested-gridding was conducted. Horizontal resolutions of $27 \times 27\,km^2$ for the largest domain, $9 \times 9\,km^2$ for the second largest domain, and $3 \times 3\,km^2$ for the smallest domain were used (Refer to Fig. 1a). In the framework, the model settings for 3 step simulations were the same, except for the biogenic emissions input. The three sets of hourly, gridded, and speciated biogenic emissions (based on KORPFT, CDP, and MODIS datasets) were merged with anthropogenic emissions (described in Sect. 2.2.2 "Anthropogenic emissions modeling").

Because we changed only PFT datasets without changing any other model input configurations, the specific simulation scenarios are hereafter referred to as KORPFT, CDP, and MODIS (Table 1).

2.2.1 Meteorological and chemical transport modeling

For meteorological inputs to the CMAQ model, MM5 modeling was carried out for a period of May–June 2008. Each of the three domains (i.e., 27 km, 9 km, and 3 km) consisted of 20 vertical layers resolving the atmosphere between the surface and 100 hPa in sigma coordinate. Applying a two-way nesting technique, the meteorological outputs from coarse-grid to fine-grid domains (i.e., 27 km to 9 km to 3 km) were derived. NCEP/DOE AMIP-II Reanalysis data (Reanalysis-2) were used for the initial and boundary conditions (IC/BC). The Grell scheme (Grell et al., 1994), based on the rate of destabilization or quasi-equilibrium, was employed for cumulus parameterization. The Medium-Range Forecast (MRF) Planetary Boundary Layer (PBL) scheme was applied to obtain high-resolution in the PBL (Hong and Pan, 1996). For an explicit

ACPD
13, 24925–24973, 2013

moisture scheme, a mixed-phase option was used (Riesner et al., 1998). In order to reduce meteorological uncertainties, four-dimensional data assimilation (FDDA) was employed with 10 m Advanced Scatterometer (ASCAT) wind data. The MM5 outputs were then processed with the Meteorology-Chemistry Interface Processor utility (Byun and Ching, 1999) to derive the meteorological input variables for CMAQ simulations.

For the O_3 air quality simulation using CMAQv4.6 (Byun and Ching, 1999; Byun and Schere, 2006), the SAPRC99 chemical mechanism for gas-phase chemistry (Carter, 2000a) and aero3 for aerosol formation (Binkowski and Roselle, 2003), the piecewise parabolic method (PPM) for advection (Collela and Woodward, 1984), multi-scale for horizontal diffusion (CMAQ v4.6 Operational Guidance Document, 2006), the Asymmetric Convective Method (ACM) for cloud (Pleim and Chang, 1992) and an updated version of ACM (ACM2) for vertical diffusion (CMAQ v4.6 Operational Guidance Document, 2006) were used. Based on these emissions and meteorological inputs, one-way nested model simulations were performed at the three domains (Fig. 1) with a 4-day spin-up period. Here, we focus on the fine and detailed domain ($3 \times 3\,km^2$) in which developed urban areas and densely-vegetated areas coexist. The BCs for the 3 km CMAQ modeling domain were obtained from the simulation outputs of the coarse domains (27 km down to 9 km) using the CMAQ BCON processor to generate hourly concentrations along the outer lateral edges of the 3 km domain. The ICs for the 3 km domain were also obtained from the CTM results at coarse domains.

2.2.2 Emissions modeling

Anthropogenic emissions modeling

For processing anthropogenic emission, SMOKE-Asia (Woo et al., 2012) was applied to generate CMAQ-ready anthropogenic emissions for our study domain. SMOKE-Asia adopts the Sparse Matrix Operator Kernel Emissions (SMOKE) processing system of the US Environmental Protection Agency (EPA) as the base frame, but with some improved and upgraded contents. For example, SMOKE-Asia includes spatial and tempo-

ACPD
13, 24925–24973, 2013

ral surrogate databases, such as 38 source classification codes (SCCs), 2752 administrative division codes, and some regionalized temporal profiles. Details of SMOKE-Asia are described in Woo et al. (2012). A merged version of the INTEX 2006 (Zhang et al., 2009) and TRACE-P 2000 inventories (Streets et al., 2003) was used as a base inventory, and was allocated into our study domain using spatial surrogates in SMOKE-Asia. Through further processing with temporal and chemical speciation (SAPRC99 chemical mechanism) profiles, we generated hourly gridded CMAQ-ready emissions data for this study.

The anthropogenic VOC and NO_x emissions processed by SMOKE-Asia for the study period are shown in Table 2, and their spatial distributions are displayed in Fig. 2.

Biogenic emissions modeling

We used the Model of Emissions of Gases and Aerosols from Nature (MEGANv2.04) (Guenther et al., 2006) to produce BVOC emission inputs to CMAQ. The BVOC flux is a function of emission factor, vegetation area, and various environmental factors:

$$\mathrm{ER} = \mathrm{EF} \cdot A \cdot \gamma_{\mathrm{F}} \cdot \gamma_{\mathrm{S}} \cdot \gamma_{\mathrm{W}} \cdot \phi, \quad (3)$$

where, ER is the net emission rate (µg of compound h^{-1}); EF is the an emission factor that represents the net in-canopy emission rate expected at standard conditions (µg m^{-2} h^{-1} at 303 K); A is the vegetation cover area represented by the PFT (A = grid area × PFTF); and γ includes environmental activity factors that account for the emission changes due to activity deviations from standard conditions, such as changes in leaf area and age (γ_{F}), stress due to soil moisture content (γ_{S}), and environmental effects (i.e., temperature and solar radiation) within the canopy (γ_{W}), and ϕ is a factor that defines chemical production and loss within plant canopies (Guenther et al., 2006).

In this study, detailed soil-moisture and plant-canopy information was not considered, so γ_{S} and ϕ were set to 1. For MEGAN utilization in this study, we only changed PFT inputs without changing any other input configurations, such as meteorological

ACPD
13, 24925–24973, 2013

and chemical variables. For EF, we applied PFT-specific emission factors tabulated in MEGAN module. For γ_W, MM5-derived solar radiation and temperature datasets were used. For the leaf area and age (γ_F) input calculation, we utilized monthly averaged LAIv data using 2008 MODIS LAI (leaf area index, 8-day coverage and 1-km resolution) and each source of PFT distribution data. In order to isolate the different impacts of each source of PFT data on the O_3 predictions, we applied those PFT datasets with a single source of LAI (i.e., MODIS LAI) rather than multiple sources of LAI data. It should be noted that the LAIv is the LAI averaged over the fraction of vegetated area.

The estimated biogenic VOC and NO emissions from the MEGAN model with the three different PFT scenarios for the study period are shown in Table 2. Overall, the biogenic VOC emissions (BVOC) contribute 44.5 % of the total VOC emissions (anthropogenic + biogenic). The inter-differences of BVOC emissions between the three PFT scenarios ranged from 1.8 Gg (MODIS-KORPFT) −4.2 Gg (MODIS-CDP) for the study period (May–June 2008). Biogenic NO_x (specifically NO) showed marginal contributions (∼ 0.4 %) to the total NO_x emissions and inter-differences (e.g., 0.02 Gg between CDP and KORPFT) between the three different PFT datasets. Investigating the distribution of the VOC/NO_x ratio across the domain revealed that consistently low values of the VOC/NO_x ratio were distributed across the domain for the case of only anthropogenic emission (i.e., $VOC/NO_x < 3$), whereas noticeably increased VOC/NO_x ratios were distributed over some suburban and border areas for the case of combined anthropogenic and biogenic emissions.

2.3 Statistical measures for quantitative evaluation

We investigated the impacts of different sources of PFT distributions on CTM O_3 predictions by examining the deviation of each dataset (i.e., PFT, BVOC emissions, and O_3) from the norm (here, their mean values). The deviation of an individual dataset at each grid cell (δGV) was calculated as follows:

$$\delta \mathrm{GV}_{X|_{(i,j)}} = \mathrm{GV}_{X|_{(i,j)}} - \overline{\mathrm{GV}_{(i,j)}}, \quad (4)$$

ACPD
13, 24925–24973, 2013

where $GV_{X|_{(i,j)}}$ is the grid cell value of an individual source of PFT X at a given grid cell location (i,j), and $\overline{GV_{(i,j)}}$ is the mean value for every source of PFT data at a given grid cell location (i,j). We consider the mean value as the best guess at what the true values of each variable (PFT areas or biogenic emissions or O_3 concentrations) were since the mean value for each set of variable data from the given scenarios describes each central tendency for those variable datasets. Beginning with a comparison of PFT area deviations, we consecutively investigated these PFT deviations on the results of MEGAN BVOC and CTM O_3 predictions. Hourly O_3, NO_x, and isoprene data gathered from the ambient air quality monitoring network, 148 ambient monitoring stations (AMS) and 8 photochemical air monitoring stations (PAMS) of the National Institute of Environmental Research were used to evaluate CMAQ O_3 predictions over the Seoul-Kyunggi Metropolitan Area for the study period.

The effect of using different PFT datasets on CTM performances was investigated based on some statistical measures: mean bias (MB); normalized mean bias (NMB); and normalized mean error (NME):

$$\text{Mean Bias (MB)} = \frac{1}{n}\sum_{i=1}^{n}(P_i - O_i), \tag{5}$$

$$\text{Normalized Mean Bias (NMB)} = \frac{\sum_{i=1}^{n}(P_i - O_i)}{\sum_{i=1}^{n} O_i} \times 100, \tag{6}$$

$$\text{Normalized Mean Error (NME)} = \frac{\sum_{i=1}^{n}|P_i - O_i|}{\sum_{i=1}^{n} O_i} \times 100, \tag{7}$$

ACPD
13, 24925–24973, 2013

where P is model prediction and O is observation.

The US EPA suggested the informal performance standards for regulatory modeling practices of ±5 to ±15 % for NMB and ±30 to ±35 % for NME (Russell and Dennis, 2000).

3 Results and discussion

3.1 Comparison of PFTs and biogenic emissions distributions

In our modeling domain, CDP (25 333 km^2) delivered the largest PFT area followed by KORPFT (25 128 km^2) and MODIS (24 101 km^2). Although the three sources of the PFT data delivered similar cover areas, clear differences were identified in the composition of the PFT classes (i.e., BT, NT, SB, and HB). For example, for BT (the major source of biogenic isoprene), MODIS (10 115 km^2) delivered the largest area followed by KORPFT (5318 km^2) and CDP (4539 km^2). For NT (the major source of biogenic terpene), KORPFT (8019 km^2) delivered the largest area followed by CDP (4967 km^2) and MODIS (1258 km^2). For SB (the second-most major source of biogenic isoprene), CDP (3920 km^2) delivered the largest area followed by KORPFT (2569 km^2) and MODIS (769 km^2). For HB (the major source of biogenic, or soil, NO), MODIS (11 959 km^2) delivered the largest area followed by CDP (11 907 km^2) and KORPFT (9223 km^2).

A comparison of the spatial patterns of the PFT area deviations allowed us to understand qualitative discrepancies among the sources of PFT data. Figure 3 shows the spatial distributions of the δPFT areas for each PFT scenario for the total vegetation and PFT classes (i.e., BT, NT, SB, and HB). The δPFT area of each PFT scenario in the study domain was produced based on Eq. (4). The resulting maps show several noticeable features in the δPFT area distributions:

1. KORPFT delivered larger BT covers over the Seoul and Incheon Metropolitan Areas, and other regions (Fig. 3b1).

ACPD
13, 24925–24973, 2013

2. KORPFT delivered larger NT covers across the domain. There are hot spots over Gangwon-do and the border areas of Gaesong and Hwanghaebuk-do (Fig. 3c1).

3. CDP lacked PFT distribution information at some islands and costal city areas off the Incheon Metropolitan Area (the brightest yellow color area in Fig. 3a2).

4. CDP delivered comparatively larger NT- and HB-type vegetation covers that concentrated in the Seoul and Incheon Metropolitan Areas and were widespread across the domain (Fig. 3a2, c2, d2, and e2) along with larger BT covers over the Gaesong and Hwanghaebukdo areas (Fig. 3b2).

5. MODIS delivered larger BT vegetation covers across the domain except for the Seoul and Incheon Metropolitan Areas and Gaeseong and some of its neighborhood areas. There are hot spots over Gangwon-do, Choongcheongbuk-do, and Choongcheongnam-do) (Fig. 3b3).

From the subsequent investigation of the δBVOC emission distributions, we found that the patterns from biogenic emission distributions closely resembled those from the PFT distributions in the study domain, except for the missing biogenic emission zones detected over the Seoul and Incheon Metropolitan Areas and some of their neighborhood areas (Fig. 4). A brief summary of the features that were similar to those from the δPFT distributions follows:

1. KORPFT estimated comparatively higher isoprene emissions from some border areas (between the Kyuggi-do and Gaesong areas and between the Kyunggi-do and Choongchongbuk-do areas) as well as some islands areas (Fig. 4b1) due to the influences of BT covers over these areas.

2. KORPFT estimated larger and widespread terpene emissions across the domain except for Seoul and some border areas, (Fig. 4c1) due to the influences of NT covers over these areas.

ACPD
13, 24925–24973, 2013

3. CDP omitted biogenic emissions from some island and costal city areas off the Incheon Metropolitan Area (Fig. 4a2, b2, c2, and d2) due to omitted PFT areas.

4. CDP estimated comparatively higher and widespread terpene and NO emissions, except for Seoul and some border areas, across the domain (Fig. 4c and d2) due to the influence of NT and HB covers, and higher isoprene emissions from the Gaesong and Hwanghaebuk-do areas (Fig. 4b2) due to the influence of BT covers.

5. MODIS estimated larger isoprene emissions across the domain except for the Seoul and Incheon Metropolitan Areas and Gaeseong and some of its neighborhood areas (Fig. 4b3) due to the influence of BT covers over these areas. There are hot spots over Gangwon-do, Choongcheongbuk-do, and Choongcheongnam-do.

The zones missing biogenic emissions (the squared zones shown with the red-dotted line in Fig. 4a–d) occurred due to missed PFT area. This artifact (i.e., PFT area missing) can occur in the process of the LAIv calculations due to the geo-locational disparity between the PFT and the LAI distributions. Biogenic emission missing due to this artifact can affect the surface-level O_3 simulation of CTM. This issue will be discussed in Sect. 3.4. Additionally, it should be noted that the BVOC emissions omitted by CDP occurred due to the fact that CDP originally did not develop PFT distributions over those areas.

The results in this section indicate that CTM O_3 predictions will vary according to the differences in the PFT distributions. In the following sections, we will discuss this issue with more detailed analyses.

3.2 PFT class-dependent BVOC emissions and their O_3-forming potentials

The links between BVOC emissions and their O_3-forming potentials (OFPs) were further investigated by focusing on the compositional differences and the OFPs of the

ACPD
13, 24925–24973, 2013

three BVOC emissions groups from the different PFT scenarios (Fig. 5). From these investigations, we found that isoprene was the most important BVOC compound showing the largest contributions to the total BVOC emission amounts and potential O_3 formation.

In the analyses, we reconstructed the 22 SAPRC99 VOC species of MEGAN into 10 BVOC compound groups for a clearer presentation of the BVOC emission distributions. The 10 reconstructed compound groups were ALKs (sum of ALK1–ALK5), AROs (sum of AROs1 and 2), CCHO (CCHO), ETHENE (ethene), HCHO (HCHO), ISOPRENE (isoprene), MEOH (MEOH), OLEs (sum of OLEs 1 and 2), Other Ox-Orgs (sum of ACET, BALD, CCO_OH, HCOOH, MEK, RCHO, and RCO_OH), and TERPENE (terpene). To examine the OFP of each PFT scenario, we employed the maximum incremental reactivity (MIR) (Carter, 2000b). The MIR is a useful quantitative measure of the impact of a VOC on O_3 under high NO_x conditions (i.e. grams of O_3 generated/grams of VOC added) under which O_3 is most sensitive to VOCs and which represent near-source or urban areas (Carter, 2000b). The MIR was derived from several box model scenarios representing various urban areas with NO_x inputs adjusted to yield maximum sensitivities of ozone to changes in VOC levels (Carter, 2000b). The MIR has been adopted in the state of California for the purpose of implementing reactivity-based regulations (CARB, 1993) and often used as a general reactivity scale to study the impact of VOC on O_3 formation (Xie et al., 2008; Zheng et al., 2009; Carter and Seinfeld, 2012).

Among the 10 BVOC compound groups, isoprene is shown to have the largest contribution to the total BVOC emissions (about 52 %) followed by MEOH, terpene, and other VOCs (Fig. 5a). Among the different PFT scenarios applied to the MEGAN biogenic emission modeling, MODIS derived the highest isoprene emissions, because of the highest BT areas, followed by KORPFT and CDP (Fig. 5b). A distinct result with the KORPFT scenario is the highest terpene emissions, shown in Fig. 5b, due to the larger NT areas of KORPFT (Fig. 3c1) compared to the other PFT scenarios.

ACPD
13, 24925–24973, 2013

By simply multiplying BVOC emissions with MIR values (Fig. 5c), we calculated domain-wide total OFPs of BVOC emissions. The calculated distributions of OFPs for each PFT scenario (Fig. 5d) were mainly affected by the spatial distributions of isoprene emissions. For example, most locations with higher OFPs were overlapped with the BT and the isoprene emission hotspots in the study domain (Figs. 3b and 4b). From the ozone forming potential computation, we derived the following proportion for the maximum O_3-forming potentials in the study domain: MODIS : KORPFT : CDP = 1 : 0.82 : 0.78. Assuming that under high NO_x level our study domain experience optimal balance between VOC and NO_x to generate O_3, this rough estimation implies that about 22 % of the maximum inter-difference in the O_3 concentrations can occur between the different PFT scenarios. For example, when the MODIS scenario estimates 60 ppb of domain average O_3 concentration, the probable O_3 concentrations from the KORPFT and CDP scenarios would be 49.2 and 46.8 ppb, respectively. There are two points to be noted here because the MIR values used for OFP calculations are from the chamber experiments (Carter, 2000b). Firstly, the proportional expression (i.e., MODIS : KORPFT : CDP = 1 : 0.82 : 0.78) we obtained were simply rough ones and it may cannot represents the relevant atmospheric conditions for O_3 formation over some areas. From Fig. 5d, we can easily recognize that the estimated proportional expression is not applicable to some areas, e.g., areas with missing BVOC reactivity zones due to the missing BVOC emissions and areas with small OFP gaps between the different PFT scenarios. Secondly, the MIR scale based OFP calculation may cannot duplicate the relevant atmospheric conditions and chemistry of VOC associated with O_3 formation for the period and domain of this study. Thus, we can only expect that the areas with higher OFP levels could have more possibility to experience higher level of O_3 formation in the presence of higher NO_x condition. This MIR-OFP application issue will be further discussed in Sect. 3.4.

Despite the mentioned limitations of MIR-OFP, this approach helps to evaluate the relative importance of biogenic VOC compounds in the production of ground-level ozone in the current study domain. In our OFP calculation, both the isoprene and

ACPD
13, 24925–24973, 2013

terpene emission amounts were the first and second largest contributors to the O_3 concentrations (about 79 % contribution by isoprene and 9 % contribution by terpene). The result suggests that the primary and secondary BVOC species of concern are isoprene and terpene because of their high reactivities and large emissions across the domain.

3.3 Relationship between PFT area deviations and CMAQ O_3 deviations

The results in Sects. 3.1 and 3.2 suggest some qualitative evidences of a causal link between the δPFT areas, δBVOC emission estimations, and the δO_3 predictions. To analyze this link more quantitatively, first-order multiple regression (MR) models that include δBT, δNT, δSB, and δHB as quantitative independent variables were fitted by the least-square method. Due to the short photochemical lifetimes of BVOC (e.g., isoprene $\sim$ 2 h) (Atkinson and Arey, 2003), the emitted BVOC from local biogenic emission sources (i.e., PFT area distributions) immediately affect the levels of local surface O_3 concentrations rather than move over long distance. The fine grid resolution system applied in this study can allow us to resolve these immediate impacts of biogenic emissions from the different sources of PFT distributions on the spatial distributions of O_3 concentrations. In this study, we assumed a linear relationship between the δPFTs and δO_3. From an analysis of the MR equations in Table 3, we could assume the expected deviations in O_3 concentration per unit change in the deviation of each individual PFT area. Furthermore, we could recognize which PFT scenario was appropriate for representing the biogenic emission capacity of the PFT distributions in our modeling domain. To explain the MR results connecting the δPFTs and δO_3, referring to the documented findings about the relative balance between VOC and NO_x can be very useful. Specifically, under VOC-limited atmospheric condition (i.e. NO_x is abundant relative to VOCs), NO_x behaves as a net O_3 inhibitor and the amount of VOC tends to limit the amount of O_3 formed. To the contrary, under a NO_x-limited condition, NO_x tends to generate O_3 and the amount of NO_x limits the amount of O_3 formed (Finlayson-Pitts and Fitts, 2000; Seinfeld and Pandis, 1998).

ACPD
13, 24925–24973, 2013

The MR for KORPFT demonstrates that gaining areas of the two major biogenic isoprene sources (i.e., $+0.016 \cdot \delta$BT and $+0.001 \cdot \delta$SB) and the one major biogenic terpene source (i.e., $+0.002 \cdot \delta$NT) contributes to O_3 increase, whereas gaining area of the major soil NO_x source (i.e., $-0.001 \cdot \delta$ HB) contributes to O_3 decrease across the domain. As an example, respective gains of BT, SB, and NT areas (Fig. 3b1, d1, and c1) can inject more isoprene and terpene species into VOC-limited regions so that those regions tend to change to the favorable condition for O_3 formation (Fig. 2d); whereas HB area gains (Fig. 3e1) feed more NO into VOC-limited regions (Fig. 2d) so that these regions tend to change slightly toward the unfavorable condition for O_3 formation. Spatially, a negative correlation ($r = -0.4$) between the δBT (Fig. 3b1) and δHB (Fig. 3e1 patterns was found across the VOC-limited regions (Fig. 2d). From the first-order MR equation for KORPFT, we can assume that unit area (here, 1 km^2) increases in BT, NT, and SB in KORPFT will lead to increases of 0.016, 0.002, and 0.001 ppb in O_3 concentration, respectively, whether the increase is from, 1 to 2 km^2 or from 10 to 11 km^2. However, every additional increase in HB area is assumed to produce a 0.001 ppb decrease in O_3 concentration (statistically significant and the most efficient model: $P<0.0001$, F value = 783, adjusted $R^2 = 0.51$, and significant parameters).

The MR for MODIS indicates positive contributions from gaining BT, SB, NT, and HB areas to O_3 increase in the domain. For example, the respective area gains for BT, SB, NT, and HB (Fig. 3b3, d3, c3, and e3) can add more isoprene, terpene, and NO into regions with the O_3-favorable condition or regions with the NO_x-limited condition (Fig. 2d), so these regions tend to become more favorable for O_3 formation. Spatially, a good negative correlation ($r = -0.53$) between the δBT (Fig. 3b3) and δHB (Fig. 3e3) patterns is found across the O_3-favored and NO_x-limited regions (Fig. 2d). From the first-order MR equation for MODIS, we can assume that a 1 km^2 increase in BT, NT, SB, and HB will lead to 0.021, 0.002, 0.006, and 0.002 ppb increases in O_3 concentration, respectively (statistically significant and the second most efficient model: $P<0.0001$, F value = 407, adjusted $R^2 = 0.35$, and significant parameters).

ACPD
13, 24925–24973, 2013

The MR for CDP suggests that gaining areas of BT and HB, respectively, contributes to increase O_3, whereas gaining NT and SB areas contributes to decrease O_3 across the domain. For instance, respective gains of BT and HB (Fig. 3b2 and e2) can inject more isoprene and NO into regions with the O_3-favorable condition (Fig. 2d), so these regions tend toward a more favorable condition for O_3 formation. However, respective gains in NT and SB can feed more terpene and isoprene into NO_x-limited regions (Fig. 2d), so these regions tend toward a more unfavorable condition for O_3 formation. No spatial correlations were found between the δPFT patterns (Fig. 3b2, c2, d2, and e2) across the O_3-favored and NO_x-limited regions. From the first-order MR equation for CDP, we can assume that a 1 km^2 increase in BT and HB will lead to 0.007 and 0.0003 ppb increases in O_3 concentration, respectively, but every additional increase in NT and SB areas is assumed to produce a 0.002 and 0.001 ppb decrease in O_3 concentration, respectively (statistically significant but inefficient model: $P<0.0001$, F value = 57, adjusted R^2 = 0.07, and partly significant parameters).

The MR analysis results quantitatively suggest that the CMAQ with KORPFT scenario can derive more accountable O_3 predictions in terms of the impacts of PFT distribution changes on surface-level O_3 changes (Adjusted R^2: KORPFT > MODIS $\gg$ CDP).

3.4 Impact of PFT distribution differences on model performance

The CMAQ-simulated O_3, NO_x, and isoprene concentrations were compared with the observed concentrations at 148 monitoring sites in the domain. Figure 6 shows a comparison between the observed and modeled O_3, NO_x, and isoprene concentrations for the period of 1 May–30 June 2008. The CMAQ predictions follow the observations reasonably well with a tendency for under-prediction for O_3 and isoprene and a tendency for over-prediction for NO_x. It should be noted that we displayed the averaged value of the CMAQ simulations with the different PFT scenarios in Fig. 6 because the time variations of the individual concentrations were not substantially separated in the graph.

ACPD
13, 24925–24973, 2013

In general, the under-predictions in O_3 concentration could primarily be caused by the combined effect of multiple sources of uncertainty, such as in O_3 precursor (e.g., NO_x and VOC) emissions, meteorological fields, and so forth. For example, an overestimation of NO_x emissions and an underestimation of VOC emissions may have contributed to the overall under-prediction of O_3 concentration under a VOC-limited condition. The over-prediction of surface wind speeds and under-prediction of ambient temperature for the simulation period may also have contributed to the O_3 under-prediction. The over-prediction of NO_x concentrations is primarily due to the overestimation of anthropogenic NO_x emissions, and the under-prediction of isoprene concentrations is due to the combined effects of the overestimations in NO_x and underestimations VOC and ambient temperature (i.e., under-predictions).

Table 4 shows a summary of the statistical measures indicating the CMAQ performance for O_3, NO_x, and isoprene for each PFT scenario at 148 monitoring sites in the domain. While the impacts of the different PFT distributions on CMAQ O_3 and NO_x performance were not readily recognized, those on CMAQ isoprene performance were clearly recognized.

For O_3, the overall evaluation statistics fall within the US EPA performance standards (i.e., ±5 to ±15 % for NMB and ±30 to ±35 % for NME), although CMAQ under-predicts against the hourly O_3 observations. Because urban sites account for about 82 % of the total datasets (121 urban sites in 148 sites) in our comparison, the under-predictions at the urban sites contribute significantly to the overall CMAQ performance, resulting in under-predictions for the 1-h average O_3 concentrations. CMAQ shows the best performance at suburban sites, followed by background, urban, and roadside. For example, the respective values of MB, NMB, and NME for 1 h average O_3 are about −0.86 ppb, −2.14 %, and 21.64 at the suburban sites, about −2.76 ppb, −5.48 %, and 22.86 % at the background sites, about −8.10 ppb, −23.49 %, and 34.60 % at the urban sites, and about −5.37 ppb, −23.17 %, and 41.02 % at the roadside sites.

Comparing the CMAQ O_3 for the three different PFT scenarios (i.e., KORPFT, CDP, and MODIS), the MODIS case provides slightly better agreement against the observa-

ACPD
13, 24925–24973, 2013

tions than the other cases. The resultant maximum O_3 inter-differences between different PFT scenarios were only 0.4 % across the monitoring sites. This is inconsistent with the MIR based OFP calculations in Sect.3.2 suggested 22 % of maximum inter-differences between the CMAQ O_3 with different PFT scenarios. This inconsistency can occur due to a couple of situations. Firstly, the O_3 simulations were conducted for the period of May–June 2008 under much narrower distributions of NO_x and temperature in the atmosphere (domain averaged NO_x range: 0–24 ppb and domain averaged temperature range: 6–26 °C) compared to those of the chamber experiment for MIR developments (chamber environment NO_x range: 150–1000 ppb and chamber experiment temperature: 22–43 °C) (Refer to Table B-1 in Carter, 2000b). This indicates that our CMAQ atmospheric conditions for photochemical O_3 formation were not fully developed to derive the maximum O_3 reactivities of BVOC emissions from different PFT scenarios. Thus, it can be said that MIR-OFP approach is crucially depend on pollution episodes (Carter and Seinfeld, 2012). Secondly, most of the urban and roadside monitoring sites coincidentally located on the missing BVOC reactivity zones (Refer to Figs. 1b and 5d). For example, 74 urban sites (in total 121 sites) and 15 roadside sites (in total 21 sites) were located on the missing BVOC reactivity zones. This indicates that the simulated O_3 over these sites were not significantly affected by different PFT scenarios. The missing BVOC reactivity problem is associated with the missing BVOC emissions which have primarily occurred due to the PFT area missing in the MEGAN biogenic emission modeling. The potential impact of this missing PFT area (or missing BVOC reactivity) on CMAQ O_3 predictions are discussed in more detail later (Refer to Table 5 and related descriptions in this section).

For NO_x, an important O_3 precursor, CMAQ over-predicts against the average value of 1 h observations for all sites, although it under-predicts at the roadside, suburban, and background sites, because of the significant contribution of the over-prediction at the urban sites to the overall performance. This inaccuracy in NO_x predictions may occur due to the effect of uncertain estimations of anthropogenic NO_x emissions, such as overestimations at the urban sites and underestimations at the other sites. The

ACPD
13, 24925–24973, 2013

respective values of MB, NMB, and NME for 1 h average NO_x are about 14.47 ppb, 40.55 %, and 71.39 % for all sites, about 19.68 ppb, 66.22 %, and 85.34 % at the urban sites, about −8.20 ppb, −9.78 %, and 59.01 % at the roadside sites, about −4.16 ppb, −31.43 %, and 63.23 % at the suburban sites, and about −12.85 ppb, −75.16 %, and 85.12 % at the background sites.

In contrast, for isoprene, another important O_3 precursor, CMAQ under-predicts against the average value of 1 h observations at PAMS distributed over urban (4 sites), suburban (3 sites), and background (1 site) areas in the domain. The respective values of MB, NMB, and NME for 1 h average isoprene are about 0.05 ppb, −21.07 %, and 63.15 % throughout all the sites. Among the three CMAQ isoprene results, the CMAQ provided values closer to the observations with MODIS (MB = −0.02 ppb and NMB = −7.78 %) than with the others (MB = −0.05 and NMB = −22.62 % with KORPFT; MB = −0.08 and NMB = −32.82 % with CDP). However, the CMAQ shows noticeably better performance for isoprene time variation with KORPFT (r = 0.622) than with the others (r = 0.598 with MODIS and r = 0.591 with CDP) (Fig. 7).

Meanwhile, we consider that the KORPFT is the representative sources of PFT data (region-specific PFT distribution dataset) in the current study domain. Why then does the CMAQ simulation with the KORPFT scenario not provide isoprene predictions that are closer to observations than those for other scenarios? We discovered a critical clue to this question from the missed PFT areas, which were briefly described in Sect. 3.1 (see Fig. 4). Table 5 shows the areas originally proposed by each PFT distribution dataset before the BVOC modeling process and the missed area (%) for each PFT distribution dataset during the BVOC emission modeling process. It is worthwhile to note that the loss of PFT areas occurs during the LAIv derivation process due to the geo-location mismatch between the PFT and the LAI distributions. The current MEGAN modeling system is designed to adopt only an external source of LAI distribution data, and no LAI distribution data source cannot beat MODIS LAI data in terms of data accessibility and user friendliness. Although PFT area loss might be inevitable at this point in time, it must be resolved in the near future to obtain more accurate biogenic emis-

ACPD
13, 24925–24973, 2013

sion and chemistry transport modeling results. The impact from the PFT distributions on ambient isoprene concentrations over the PAMS sites is probably underestimated slightly in CMAQ with some missed isoprene emissions. Across the PAMS sites, the KORPFT scenario missed a larger isoprene emission source area (i.e., BT) than those of other PFT scenarios by factors of 3 to 18. For example, KORPFT missed about 4.73 km^2, CDP missed about 0.26 km^2, and MODIS missed about 1.49 km^2 of BT area across the PAMS sites. This finding indicates the possibility that CMAQ-KORPFT with a consideration of the missed BT area can predict isoprene concentrations much closer to the observations at the PAMS sites. Furthermore, this analysis suggests that change of BT areas can significantly affect CMAQ isoprene predictions.

In the same way, the relatively poor CMAQ O_3 performances at the urban and road sites can be analyzed. Of the O_3 monitoring sites, the urban sites (missed 80–505 km^2) underwent the biggest loss of PFT area followed by the roadside (missed 7–95 km^2) and the background sites (missed 3–7 km^2). However, the suburban sites maintained the original PFT without any loss of PFT area. These PFT area losses can partly contribute to underestimation of biogenic emissions and, subsequently, affect CMAQ O_3 prediction results at the monitoring sites (e.g., under-predictions of urban and roadside O_3 concentrations). In addition, underestimation of BVOC emissions due to the PFT losses is likely to impact the CMAQ NO_x prediction result at the urban sites. For example, higher concentrations of the peroxy radical in the BVOC oxidation cycle in the urban atmosphere convert more NO to NO_2 in a fast and efficient manner through the radical transfer reaction (i.e., $RO_2^{\bullet} + NO \rightarrow NO_2 + RO^{\bullet}$). Then, the hydroxyl radical transforms the converted NO_2 to nitric acid (i.e., $NO_2 + OH + M \rightarrow HNO_3 + M$). Eventually, the urban atmosphere can have a greater possibility of decreases in CMAQ NO_x concentrations.

Further analysis of the missed PFT area data with the MR equations in Table 4 allowed us to roughly assume the impact from the missed PFT area on the CMAQ O_3 predictions. For example, substituting the missed PFT areas of KORPFT into the MR equation (i.e., δBT = 66.28, δNT = 34.92, δSB = 10.35, and δHB = 40.75) yields

ACPD
13, 24925–24973, 2013

1.14 ppb of O_3 concentration loss at the urban sites. In the same way, we can estimate the missed O_3 concentrations for CDP (0.20 ppb of O_3 gain at the urban sites) and MODIS (0.54 ppb of O_3 loss at the urban sites). At all of the O_3 monitoring sites, the missing O_3 concentrations due to the PFT area losses for the KORPFT, CDP, and MODIS scenarios are 1.29 ppb, −0.24 ppb, and 0.59 ppb, respectively. Adding each of these missing O_3 concentrations to the corresponding CMAQ O_3 values in Table 4 resulted in decreased MB values for KORPFT (−4.47 ppb → −3.18 ppb) and MODIS (−4.39 ppb → −3.80 ppb), whereas CDP MB value increased (−4.50 ppb → −4.75 ppb). This analysis suggests that deviations of BT areas can significantly affect CMAQ O_3 predictions.

3.5 Impact of PFT distribution differences on hourly O_3 predictions

From the investigation of the day-time O_3 episodes, we found noticeable deviation patterns of hourly CMAQ O_3 predictions with different PFT scenarios in our modeling domain. Figure 8a and b show the time change of the spatial distributions of δO_3 and mean O_3 concentrations in the surface layer for daytime of 29 May 2008 and 30 June 2008, respectively. The δO_3 distributions were produced by subtracting the hourly CMAQ O_3 distributions for each scenario (i.e., KOROFT, CDP, and MODIS) from the average of these three CMAQ O_3 distributions (see Eq. 4). The δO_3 distributions show that MODIS usually develops higher positive deviations (Fig. 8a11–a15 and 8b11–b15) while CDP usually develops higher negative O_3 deviations (Fig. 8a6–a10 and 8b6–b10) across the domain. The KORPFT develops both negative and positive O_3 deviations (Fig. 8a1–a5 and b1–b5) across the domain. Interestingly, the patterns of these negative or positive O_3 deviations develop in concert with enhancements in ambient O_3 concentration.

The 29 May 2008 episode shows relatively high concentrations of the simulated O_3 over some island and costal city areas off the Incheon Metropolitan Area. At the time, the Incheon coastal and neighborhood areas were located downwind of the Incheon industrial complex and the Kyunggi-do and Seoul Metropolitan Areas, where anthro-

ACPD
13, 24925–24973, 2013

pogenic NO_x emissions are very strogn (emission ratio for VOC / NO_x < 3, see Fig. 2d), and suffered a temperature inversion that limited the vertical mixing of pollutants (see the grey-hatched zones in Fig. 8a). While the released BVOC was trapped within the inversion layer, the easterly winds brought anthropogenic NO_x-rich air from the Incheon industrial complex and some areas further inland (e.g., Kyunggi-do and Seoul) to the inversion area. With the temperature inversion, mixing between the local BVOC emissions and the intruded anthropogenic NO_x and VOC produced high concentrations of O_3 through the photochemical reaction. Eventually, the Incheon coastal and neighborhood areas suffered consistently high O_3 development. The most distinctive feature of the δO_3 pattern on 29 May 2008 is the deviations of O_3 (maximum inter-difference is up to 7 ppb: 3 ppb of δO_3 for MODIS and −4 ppb of δO_3 for CDP at 15:00 p.m.) that developed and consistently remained in the temperature inversion zone (i.e., the Incheon coastal and neighborhood areas). The location of this deviation is coincident with the location of the PFT deviation in Fig. 3 and the BVOC deviation in Fig. 4. The high negative deviation of CDP O_3 is associated with the influence of the missing PFT areas of CDP (see Fig. 3a2, b2, c2, d2, and e2) on the CMAQ O_3 predictions over these areas. The high positive deviation of O_3 with the MODIS scenario is associated with the impact of the larger PFT areas (e.g., δBT ∼ 1.5 km^2 and δNT ∼ 2.1 km^2) of MODIS on the CMAQ predictions over the area (see Fig. 3b3 and c3, Fig. 4b3 and c3, and Fig. 5b).

The 30 June 2008 episode shows more widespread concentrations of the simulated O_3 throughout the domain. At the time, most of the high O_3 concentration regimes (e.g., see the O_3 contour in Fig. 8b3–b4) were located downwind from higher anthropogenic NO_x emission source areas (Fig. 2a). The anthropogenic NO_x emissions transported from urban center areas affected several border areas (e.g., the border areas between Seoul and Kyunggi-do, between Kyunggi-do and Gaeseong, between Kyunggi-do and Gangwon-do, and between Kyunggi-do and Choongcheongnam-do and Choongcheongbuk-do, etc.) and some suburban areas (e.g., the southern part of Kyunggi-do and the northern part of Choongcheongnam-do) where abundant hy-

ACPD
13, 24925–24973, 2013

droperoxy and organic peroxy radicals are generated through the oxidation of large amounts of locally emitted BVOC, resulting in high O_3 concentrations upon photolysis. Although the Incheon coastal area and the neighborhood areas underwent a temperature inversion similar to the 29 May 2008 episode, these areas were not consistently affected by anthropogenic NO_x transported from inland areas due to a wind direction change (i.e., easterly to westerly). One of the most noticeable features of the δO_3 pattern for 30 June 2008 is the strong deviations of O_3 that develop over Gangwon-do (inter-difference is up to 10 ppb: −4 ppb of δO_3 for KORPFT and 6 ppb for MODIS) and Choongcheongbuk-do (inter-differences of 9–10 ppb: −4 ppb of δO_3 for KORPFT, −3 ppb for CDP, and 6 ppb for MODIS) at 17:00 p.m. Another noticeable feature is the consistent deviations, which are not small, (inter-difference up to 5 ppb: ∼ −2 ppb of δO_3 for CDP and ∼ 3 ppb for MODIS) that develop over the border areas between East Seoul and Kyunggi-do. Figures 3 and 5 show that these higher O_3 deviations are associated with higher deviations in biogenic isoprene emissions that occur due to the higher inter-difference of BT area among the different PFT scenarios (e.g., the positive δBT area of MODIS (∼ 3.5 km^2) and the negative δBT areas of other PFTs (∼ −3 km^2)).

Interestingly, the 9–10 ppb of inter-difference between CMAQ O_3 with the different scenarios, detected in the 30 June 2008 episode, is about 11 % (i.e., [10 ppb of CMAQ O_3 inter-difference]/[90 ppb of CMAQ O_3] × 100) by percentage. This corresponds roughly to half of the maximum inter-difference (i.e., 22 %) estimated based on application of the MIR-OFP approach in Sect. 3.2. As mentioned earlier in Sect. 3.4, this gap could be the result of differences between the assumed CMAQ atmospheric conditions for surface level O_3 prediction and the chamber simulation conditions for MIR estimation. The earlier discussions regarding MIR-OFP and the results in this section can provide important implications to air quality supporting groups of the municipal governments for designing and implementing biogenic emission estimation and air quality management strategies in this region (the Seoul, Kyunggi and Incheon Metropolitan Areas). For example, as described in the literatures (Zheng et al., 2009; Carter and Seinfeld, 2012), the distributions of MIRs-OFPs for BVOC compounds can be affected

ACPD
13, 24925–24973, 2013

more dynamically by the meteorological factors (e.g. wind direction, temperature, light intensity, etc.) and the locations and magnitudes of source emissions in this region. This discussion points out that developing region-specific reactivity scale for BVOC can be an important tool to better characterize the impact of ozone precursor emissions on regional ozone formation mechanisms and support the O_3 air quality management strategies in this region. In this sense, accurate BVOC inventory based on the representative PFT information would be an essential prerequisite to yield appropriate MIR-OFP information in this region.

In addition, the resultant high inter-differences in the CMAQ 1 h O_3 predictions with the different PFT scenarios could have important implications for air quality decisions and human health studies. For example, the Korea O_3 alert system provides a warning at 120 ppb and an alarm at 300 ppb for 1 h O_3, and the Korea NAAQS (national ambient air quality standard) values for 1 h O_3 and 8 h O_3 are 100 ppb and 60 ppb, respectively. In the short term, the highly biased forecasting (e.g., bias up to 10 ppb) of high O_3 episodes may result in the incorrect issuance of O_3 alerts. Moreover, such inaccurate mean O_3 forecasting may result in the suggestion of incorrect regulatory design values to O_3 air-quality decision supporting authorities. Ji et al. (2011) reported that emergency hospitalizations for total respiratory disease increased by about 3 % per 10 ppb 24 h O_3 among the elderly. This result suggests a critical point at which chemistry transport modeling with highly biased PFT distribution scenarios would predict highly biased O_3 concentrations and subsequently provide misleading information for studying the relationship between O_3 air quality and human health outcomes.

Another point of concern is the impact from uncertain meteorological variables, especially temperature. Figure 8 shows the deviation tendencies of the simulated BVOC emissions and O_3 concentrations as a function of temperature for the three different PFT scenarios. KORPFT shows a comparatively gentle declining tendency for both δBVOC and δO_3 whereas the other two PFT scenarios show steeper inclining (MODIS) and declining (CDP) tendencies for both δBVOC and δO_3 as temperature increases.

ACPD
13, 24925–24973, 2013

These results indicate that the reliability of KORPFT should allow it to provide less biased information on the biogenic emission capacity of the plants in the study domain.

These diverging tendencies can be expected to be increase (especially for MODIS and CDP) as the weather warms due to the seasonal change from early summer to mid-summer. Assuming ambient temperature increases due to climate forcing in the future (IPCC, 2007), the use of a correct source of PFT data becomes more critical in terms of whether uncertainties in O_3 prediction results would be mild or severe.

4 Conclusions

From the investigation of the δPFT areas and δBVOC emission distributions for each PFT scenario (KORPFT, CDP, and MODIS), similar patterns were clearly shown for the PFT and BVOC emission distributions. Three PFT scenarios commonly showed that broadleaf trees (BT) were the most significant contributor, followed by needleleaf trees (NT), shrub (SB), and herbaceous plants (HB), to the total BVOC emissions. Furthermore, isoprene from BT and terpene from NT were recognized as significant primary and secondary BVOC species of interest in terms of potential O_3 level increases in the study domain.

Multiple regression analyses (CMAQ δO_3 results vs. δPFT variable datasets) with the different PFT scenarios suggested that the region-specific PFT distribution dataset (i.e., KORPFT) provides better explanations for the relationship between PFT, BVOC emission and surface-level O_3 changes. An analysis of the CMAQ performance with the different PFT scenarios suggested that deviations of broadleaf areas between different PFT scenarios can significantly affect the performance of CMAQ for O_3 and its precursors (e.g., isoprene). After further evaluation of CMAQ isoprene and O_3 predictions at the urban sites, we discovered that the large PFT area loss problem that can occur due to the geo-locational mismatch of the PFT and LAI distributions can cause increased bias in O_3 simulations. Thus, we suggest that this PFT distribution data loss artifact must be recognized as a limitation of MEGAN biogenic emission modeling and

ACPD
13, 24925–24973, 2013

chemistry transport model O_3 simulations at this point in time and must be resolved in the near future.

The temporally and spatially averaged effects of the different PFT distributions on CMAQ O_3 simulation results can be regarded as marginal because the usual inter-difference of CMAQ O_3 simulations with different PFT scenarios is less than 0.4 ppb. However, the hourly and local impacts of these are quite noticeable, showing occasional inter-differences of O_3 of up to 10 ppb.

Exponentially diverging hourly BVOC emissions and O_3 concentrations were found as a function of temperature change in our modeling domain. Thus, we conclude that the PFT distributions could play the role of a large uncertainty source in hourly O_3 air quality modeling (or forecasting) in support of air quality decision-making and human health studies. The higher the ambient temperature applied to air quality simulation, the larger the bias likely bias related to PFT distributions.

Based on the findings and conclusions presented here, we suggest that the use of representative PFT distribution data can provide less biased results in regional or local biogenic emission and photochemical O_3 predictions and that other sources of PFT distribution data (e.g., MODIS) can serve as an alternative.

Acknowledgements. This subject is supported by the Korea Ministry of Environment as "The Eco-Innovation project."" Also, this work is supported by Korea Minister of Ministry of Land, Infrastructure, and Transport as "The U-City Master and Doctor Course Grant Program." MODIS landcover (MCD12Q1) and LAI (MCD15A2) data were obtained through the online data pool at the NASA Land Processes Distributed Active Archive Center (LP DAAC).

References

Arneth, A., Schurgers, G., Lathiere, J., Duhl, T., Beerling, D. J., Hewitt, C. N., Martin, M., and Guenther, A.: Global terrestrial isoprene emission models: sensitivity to variability in climate and vegetation, Atmos. Chem. Phys., 11, 8037–8052, doi:10.5194/acp-11-8037-2011, 2011.

Atkinson, R. and Arey, J.: Gas-phase tropospheric chemistry of biogenic volatile organic compounds: a review, Atmos. Environ., 37 (Suppl. 2), The 1997 Southern California Ozone Study

ACPD

13, 24925–24973, 2013

(SCOS97-NARSTO). Dedicated to the Memory of Dr. Glen Cass (1947–2001), S197–S219, 2003.
Binkowski, F. S. and Roselle, S. J.: Models-3 Community Multi-scale Air Quality (CMAQ) model aerosol components: 1. model description, J. Geophys. Res., 108, 4183, doi:10.1029/2001JD001409, 2003.
Bonan, G. B., Levis, S., Kergoat, L., and Oleson, K. W.: Landscapes as patches of plant functional types: An integrating concept for climate and ecosystem models, Global Biogeochem. Cy., 16(2), 5.1–5.23, doi:10.1029/2000GB001360, 2002.
Byun, D. W. and Ching, J. K. S.: Science algorithms of the EPA models-3 Community Multiscale Air Quality (CMAQ) modeling system, EPA/600/R-99/030, US EPA, Research Triangle Park, USA, 1999.
Byun, D. W. and Schere, K. L.: Review of the Governing Equations, Computational Algorithms, and Other Components of the Models-3 Community Multiscale Air Quality (CMAQ) Modeling System, Appl. Mech. Rev., 59, 51–77, 2006.
CARB, Proposed Regulations for Low-Emission Vehicles and Clean Fuels – Staff Report and Technical Support Document, California Air Resources Board, Sacramento, CA. 1993.
Carter, W. P. L.: Implementation of the SAPRC-99 chemical mechanism into the models-3 framework. Report to the United States Environmental Protection Agency, 2000a.
Carter, W. P. L.: Documentation of the SAPRC-99 Chemical Mechanism for VOC Reactivity Assessment," Report to the California Air Resources Board, Contracts 92–329 and 95–308, (http://cert.ucr.edu/~carter/absts.htm#saprc99) 8 May, 2000b.
Carter, W. P. L.: Research on Atmospheric Chemical Mechanisms and VOC Reactivity, Prepared for the International Meeting: VOC reactivity and strategies for Ozone control São Paulo, (http://www.cepema.usp.br/wp-content/uploads/2009/12/Paper_Research-on-Atmospheric-Chemical-Mechanisms-and-VOC-Reactivity_WPL-Carter.pdf), Brazil 26 September, 2009.
Carter, W. P. L. and Seinfeld, J. H.: Winter ozone formation and VOC incremental reactivities in the Upper Green River Basin of Wyoming, Atmos. Environ., 50, 255–266, 2012.
Chameides, W., Lindsay, R., Richardson, J. and Kiang, C.: The role of biogenic hydrocarbons in urban photochemical smog: Atlanta as a case study, Science, 241, 1473–1475, 1988.
CMAQ v4.6 Operational Guidance Document, (http://www.ie.unc.edu/cempd/products/cmaq/op_guidance_4.6/html), 2006.

ACPD
13, 24925–24973, 2013

Colella, P. and Woodward, P. L.: The Piecewise Parabolic Method (PPM) for gas dynamical simulation, J. Comput. Phys., 54, 174–201, 1984.
Finlayson-Pitts, B. J. and Pitts Jr., J. N.: Chemistry of the Upper and Lower Atmosphere: Theory, Experiments and Applications, Academic Press, San Diego, 2000.
Friedl, M. A., McIver, D. K., Hodges, J. C. F., Zhang, X. Y., Muchoney, D., Strahler, A. H., Woodcock, C. E., Gopal, S., Schneider, A., Cooper, A., Baccini, A., Gao, F., and Schaaf, C.: Global Land Cover Mapping from MODIS: Algorithms and Early Results, Remote Sens. Environ., 83, 287–302, 2002.
Grell, G. A., Dudhia, J., and Stauffer, D. R.: A description of the fifth-generation Penn State/NCAR mesoscale model (MM5), NCAR Technical Note, NCAR/TN-398+STR, 117, 1994.
Guenther, A., Karl, T., Harley, P., Wiedinmyer, C., Palmer, P. I., and Geron, C.: Estimates of global terrestrial isoprene emissions using MEGAN (Model of Emissions of Gases and Aerosols from Nature), Atmos. Chem. Phys., 6, 3181–3210, doi:10.5194/acp-6-3181-2006, 2006.
Hogrefe, C., Isukapalli, S., Tang, X., Georgopoulos, P., He, S., Zalewsky, E., Hao, W., Ku, J., Key, T., and Sistla, G.:, Impact of biogenic emission uncertainties on the simulated response of ozone and fine Particulate Matter to anthropogenic emission reductions, J. Air Waste Manag. Assoc., 61, 92–108, 2011.
Hong, S.-Y. and Pan, H.-L.: Nonlocal boundary layer vertical diffusion in a medium-range forecast model, Mon. Weather Rev., 124, 2322–2339, 1996.
IPCC Climate Change 2007: The Physical Science Basis, Contribution of Working Group I to the Fourth Assessment Report of the Intergovernmental Panel on Climate Change, edited by: Solomon, S., Qin, D., Manning, M., Chen, Z., Marquis, M., Averyt, K. B., Tignor, M., and Miller, H. L., Cambridge University Press, Cambridge, UK and New York, NY, USA, 996 pp., 2007.
Ji, M., Cohan, D. S., and Bell, M. L.: Meta-analysis of the association between short-term exposure to ambient ozone and respiratory hospital admissions, Environ. Res. Lett., 6, 024006, doi:10.1088/1748-9326/6/2/024006, 2011.
Ministry of Environment: Environmental Review 2011, (http://eng.me.go.kr/file.do?method=fileDownloader&attachSeq=3289), 2012a.
KEI (Korea Environment Institute) and (KOSAE) Korean Society for Atmospheric Environment: Establishment of the mid/long-term directions of air quality management plan in the Seoul

ACPD
13, 24925–24973, 2013

Metropolitan Areas (SMA), Report to the Metropolitan Air Quality Management Office, Korea, September 2012.
Ministry of Environment: Annual Report of Ambient Air Quality in Korea, 2012b.
Pfister, G. G., Emmons, L. K., Hess, P. G., Lamarque, J. F., Orlando, J. J., Walters, S., Guenther, A., Palmer, P. I., and Lawrence, P. J.: Contribution of isoprene to chemical budgets: A model tracer study with the NCAR CTM MOZART-4, J. Geophys. Res., 113, D05308, doi:10.1029/2007JD008948, 2008
Pleim, J. E. and Chang, J. S.: A non-local closure model in the convective boundary layer, Atmos. Environ., 26A, 965–981, 1992.
Reisner, J., Rasmussen, R. J., and Bruintjes, R. T.: Explicit forecasting of supercooled liquid water in winter storms using MM5 mesoscale model, Q. J. Roy. Meteor. Soc., 124B, 1071–1107, 1998.
Russell, A. G. and Dennis, R.: NARSTO critical review of photochemical models and modeling, Atmos. Environ., 34, 2284–2324, 2000.
Seinfeld, J. H. and P. J. Pandis: Atmospheric Chemistry and Physics: From Air Pollution to Climate Change, John Wiley, New York, 1998.
Strahler, A., Muchoney, D., Borak, J., Friedl, M. A., Gopal, S., Lambin, E., and Moody, A.: MODIS land cover product algorithm theoretical basis document (ATBD) (Version 5.0), 1999 (http://modis.gsfc.nasa.gov/data/atbd/atbd_mod12.pdf).
Streets, D. G., Bond, T. C., Carmichael, G. R., Fernandes, S. D., Fu, Q., He, D., Klimont, Z., Nelson, S. M., Tsai, N. Y., Wang, M. Q., Woo, J.-H., and Yarber, K. F.: An inventory of gaseous and primary aerosol emissions in Asia in the year 2000, J. Geophys. Res., 108, 8809, doi:10.1029/2002JD003093, 2003.
Sun, W., Liang, S., Xu, G., Fang, H., and Dickinson, R.: Mapping plant functional types from MODIS data using multisource evidential reasoning, Remote Sens. Environ., 112, 1010–1024, 2008.
Tao, Z., Larson, S. M., Wuebbles, D. J., Williams, A., and Caughey, M.: A Summer Simulation of Biogenic Contributions to Ground-Level Ozone over the Continental United States, J. Geophys. Res., 108, 4404, doi:10.1029/2002JD002945, 2003.
Woo, J.-H., Choi, K.-C., Kim, H.-K., Baek, B. H., Jang, M. D., Eum, J.-H., Song, C. H., Ma, Y.-I., Young Sunwoo, Y., Chang, L.-S., and Yoo, Y. H.: Development of an anthropogenic emissions processing system for Asia using SMOKE, Atmos. Environ., 58, 5–13, 2012.

ACPD
13, 24925–24973, 2013

Xie, X., Shao, M., Liu, Y., Lu, S. H., Chang, C. C., and Chen, Z. M.: Estimate of initial isoprene contribution to ozone formation potential in Beijing, China, Atmos. Environ., 42, 6000–6010, 2008.

Zhang, Q., Streets, D. G., Carmichael, G. R., He, K. B., Huo, H., Kannari, A., Klimont, Z., Park, I. S., Reddy, S., Fu, J. S., Chen, D., Duan, L., Lei, Y., Wang, L. T., and Yao, Z. L.: Asian emissions in 2006 for the NASA INTEX-B mission, Atmos. Chem. Phys., 9, 5131–5153, doi:10.5194/acp-9-5131-2009, 2009.

Zheng, J. Y., Shao, M., Che, W. W., Zhang, L. J., Zhong, L. J., Zhang, Y. H., and Streets, D. G.: Speciated VOC emission inventory and spatial patterns of ozone formation potential in the Pearl River Delta, China, Environ. Sci. Technol., 43, 8580–8586, 2009.

ACPD
13, 24925–24973, 2013

Table 1. List of model simulation scenarios and the PFT datasets used for biogenic emissions modeling.

Simulation name	D1 (27 km)	D2 (9 km)	D3 (3 km)
KORPFT	MODIS	KORPFT	KORPFT
CDP	MODIS	CDP	CDP
MODIS	MODIS	MODIS	MODIS

ACPD
13, 24925–24973, 2013

Table 2. Anthropogenic and biogenic NMVOC and NO_x emissions and deviations between different PFT-input cases (Unit: Gg period^{-1}).

	Anthropogenic	Biogenic emissions						
	emissions	Mean	KORPFT	CDP	MODIS	δKORPFT	δCDP	δMODIS
NMVOC	37.24	29.83	29.98	27.68	31.83	0.15	−2.15	2.00
NO_x	43.37	0.18	0.17	0.19	0.18	−0.01	0.01	0.00

ACPD
13, 24925–24973, 2013

Table 3. The relationship between O_3 deviations and the corresponding PFT area deviations across the domain ($\delta O_3 = a \cdot \delta BT + b \cdot NT + c \cdot \delta SB + d \cdot \delta HB + e$). The second to sixth columns show the estimated coefficients of the explanatory variables and the intercept of the regression model. The seventh column shows the adjusted coefficient of determination representing the explanation power of the multiple regression model. The eighth and the ninth columns show test statistics for the regression model. A higher F statistic and a lower P value indicates greater significance of the regression model. The tenth column shows the number of datasets used in the statistical fitting. The significance levels based on the t-statistic are (***) for 0.001, (**) for 0.01, (*) for 0.05, (.) for 0.1, and () for 1.

PFT Scenario	Parameters					Adjusted-R^2	P value	F statistic	n
	a	b	c	d	e				
KORPFT	0.016 (***)	0.002 (***)	0.001 (**)	−0.001 (***)	−0.015 (***)	0.51	<0.0001	783	2978
MODIS	0.021 (***)	0.002 (*)	0.006 (***)	0.002 (**)	0.056 (***)	0.35	< 0.0001	407	2978
CDP	0.007 (***)	−0.002 (*)	−0.001 (.)	0.0003 ( )	−0.051 (***)	0.07	<0.0001	57	2978

ACPD
13, 24925–24973, 2013

Table 4. Performance statistics for CMAQ O_3 with the three different BVOC emission scenarios against the measured O_3 concentrations.

	Mean (ppb)				MB (ppb)			NMB (%)			NME (%)			Correlation coeff.		
	Obs.	KORPFT	CDP	MODIS	KORPFT	CDP	MODIS	KORPFT	CDP	MODIS	KORPFT	CDP	MODIS	KORPFT	CDP	MODIS
O_3 (Overall 148 sites, Urban 121 sites, Roadside 18 sites, Suburban 6 sites, Background 3 sites)																
Overall	30.16	25.69	25.66	25.77	−4.47	−4.50	−4.39	−14.82	−14.92	−14.56	29.54	29.54	29.53	0.740	0.740	0.739
Urban	34.49	26.37	26.32	26.47	−8.12	−8.17	−8.02	−23.54	−23.68	−23.25	34.61	34.58	34.62	0.671	0.672	0.670
Roadside	24.75	19.00	18.97	19.07	−5.75	−5.77	−5.68	−23.23	−23.33	−22.96	41.00	40.99	41.07	0.658	0.659	0.657
Suburban	40.24	39.35	39.31	39.46	−0.88	−0.92	−0.78	−2.19	−2.29	−1.94	21.63	21.67	21.63	0.790	0.789	0.788
Background	50.43	47.67	47.59	47.73	−2.76	−2.83	−2.69	−5.47	−5.62	−5.34	22.86	22.84	22.87	0.494	0.495	0.493
NO_x (Overall 148 sites, Urban 121 sites, Roadside 18 sites, Suburban 6 sites, Background 3 sites)																
Overall	35.69	50.15	50.16	50.15	14.47	14.48	14.46	40.54	40.57	40.53	71.38	71.39	71.38	0.539	0.539	0.539
Urban	29.71	49.39	49.40	49.38	19.67	19.68	19.67	66.21	66.25	66.20	85.33	85.34	85.33	0.567	0.567	0.567
Roadside	83.82	75.62	75.63	75.61	−8.20	−8.19	−8.21	−9.79	−9.77	−9.79	59.01	59.01	59.01	0.264	0.264	0.264
Suburban	13.25	9.08	9.10	9.08	−4.17	−4.15	−4.17	−31.46	−31.35	−31.49	63.26	63.20	63.23	0.320	0.320	0.320
Background	17.10	4.25	4.25	4.25	−12.85	−12.86	−12.85	−75.15	−75.17	−75.17	85.10	85.14	85.11	N.C.	N.C.	N.C.
Isoprene (PAMS 8 sites)																
PAMS	0.23	0.18	0.15	0.21	−0.05	−0.08	−0.02	−22.62	−32.82	−7.78	60.98	63.69	64.78	0.622	0.591	0.598

N.C.: not correlated.

ACPD
13, 24925–24973, 2013

Table 5. Proposed vegetation areas by PFT dataset and area loss due to the geo-location disagreement between PFT and LAI data at each grid cell.

	PFT area proposed (km^2)			PFT area loss (%)		
	KORPFT	CDP	MODIS	KORPFT	CDP	MODIS
	Overall (148 sites)					
BT	114.92	29.98	89.44	65.33	20.41	23.48
NT	127.81	127.44	37.05	32.00	51.28	30.89
SB	37.41	325.71	47.26	32.70	64.75	36.13
HB	188.31	555.35	216.30	25.34	57.25	18.87
Total	468.44	1038.48	390.04	37.56	57.81	23.16
	Urban (121 sites)					
BT	94.75	21.47	56.39	69.95	27.15	35.42
NT	92.62	100.39	24.31	37.71	56.95	32.30
SB	28.58	272.33	42.54	36.22	64.73	34.64
HB	154.60	468.10	185.69	26.36	56.77	19.98
Total	370.55	862.29	308.93	41.10	58.57	25.79
	Roadside (18 sites)					
BT	9.69	2.94	8.10	81.79	9.86	12.69
NT	7.90	10.86	1.70	52.42	75.32	95.76
SB	2.92	40.29	1.18	43.96	85.98	79.80
HB	10.19	64.84	11.64	30.02	80.46	31.95
Total	30.70	118.93	22.62	53.46	80.11	32.34
	Suburban (6 sites)					
BT	8.82	5.57	21.33	0.00	0.00	0.00
NT	15.82	11.57	5.38	0.00	0.00	0.00
SB	5.20	11.14	1.35	0.00	0.00	0.00
HB	14.47	21.13	15.67	0.00	0.00	0.00
Total	44.32	49.41	43.73	0.00	0.00	0.00
	Background (3 sites)					
BT	1.65	0.00	3.62	52.70	0.00	0.00
NT	11.47	4.62	5.66	16.02	0.00	34.69
SB	0.70	1.95	2.19	84.59	0.00	64.03
HB	9.05	1.29	3.30	43.22	0.00	0.00
Total	22.87	7.86	14.76	31.53	0.00	22.78
	PAMS (8 sites)					
BT	10.08	3.24	12.15	46.92	8.04	12.24
NT	11.19	12.52	7.56	33.88	27.39	35.07
SB	3.61	16.11	2.91	34.71	46.92	70.70
HB	14.59	22.89	9.11	48.53	49.84	21.42
Total	39.47	54.76	31.72	42.70	41.38	25.67

ACPD
13, 24925–24973, 2013

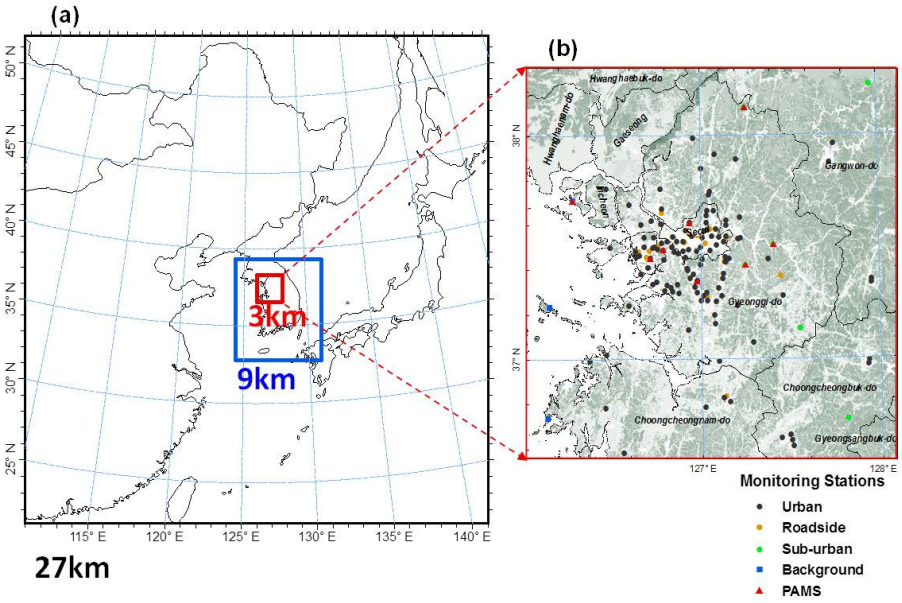

Fig. 1. The modeling domain. The target domain is a $3 \times 3\,km^2$ grid system domain covering the Seoul, Kyunggi, and Incheon Metropolitan Areas.

ACPD
13, 24925–24973, 2013

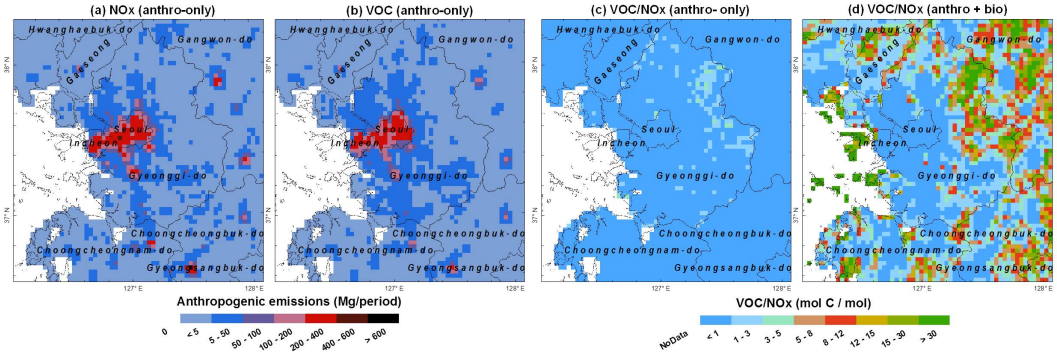

Fig. 2. Geospatial distributions of estimated anthropogenic emissions for NO_x and VOCs and their ratios for the study period (May–June 2008). The VOC / NO_x ratio for the "anthro-only" case includes only the anthropogenic VOCs and NO_x emissions; the "anthro + bio" case includes both the anthropogenic and biogenic VOCs and NO_x emissions.

ACPD
13, 24925–24973, 2013

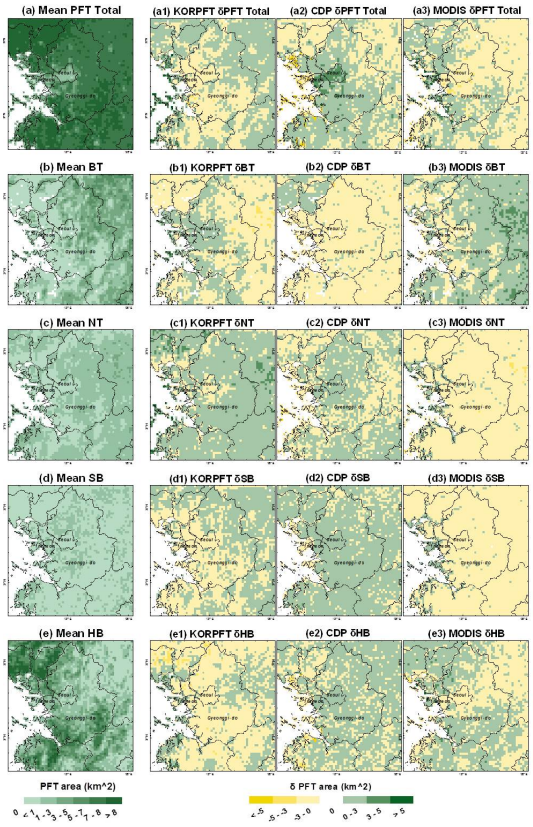

Fig. 3. Spatial distribution of the PFT area deviations for each PFT scenario. The mean spatial distributions for PFT total and the PFT classes (BT, NT, SB and HB) were derived by averaging the three different distribution data sources.

ACPD
13, 24925–24973, 2013

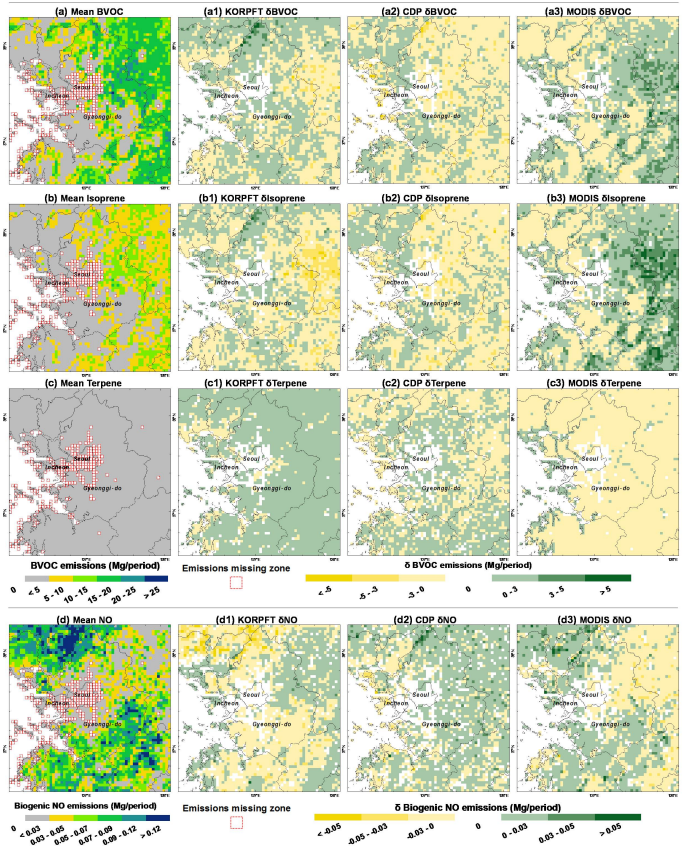

Fig. 4. Spatial distribution of biogenic emission deviations for each PFT scenario. The red-dotted squares denote the zones missing biogenic emissions during the MEGAN emission modeling.

ACPD
13, 24925–24973, 2013

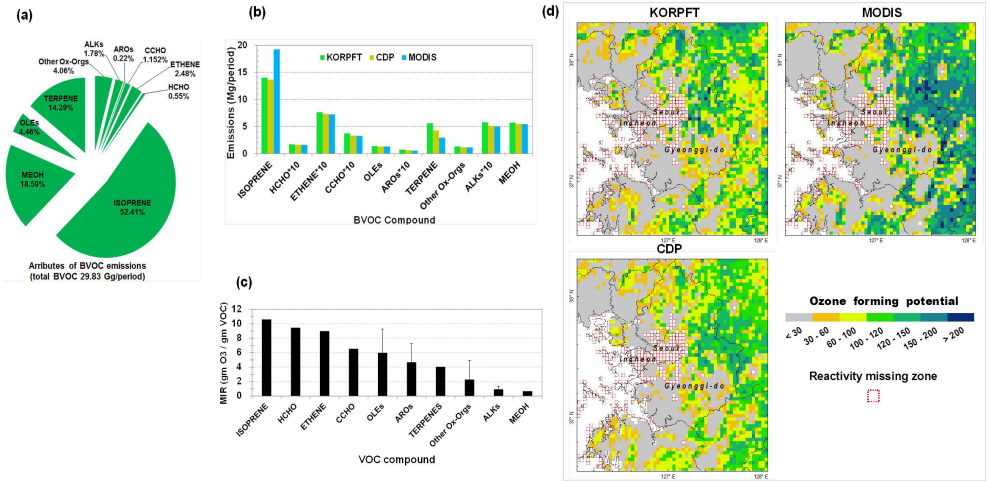

Fig. 5. Composition and distribution of the estimated BVOC emissions, along with spatial distribution of the estimated net ozone forming potentials of biogenic VOC emissions. The total BVOC in **(a)** was derived by averaging the total BVOC emissions of the three sources of data. The 10 BVOC compound groups in **(b)** are arranged in descending order following their O_3 reactivity, i.e., MIR shown in **(c)**. The distributed net ozone forming potentials in **(d)** were calculated by aggregating the O_3-forming potentials (OFPs) for 10 BVOC compound groups calculated by multiplying the emissions by their corresponding MIR values at each grid cells. The red- dotted squares denote the zones missing BVOC reactivity due to the missing biogenic emissions during the OFP calculations.

ACPD
13, 24925–24973, 2013

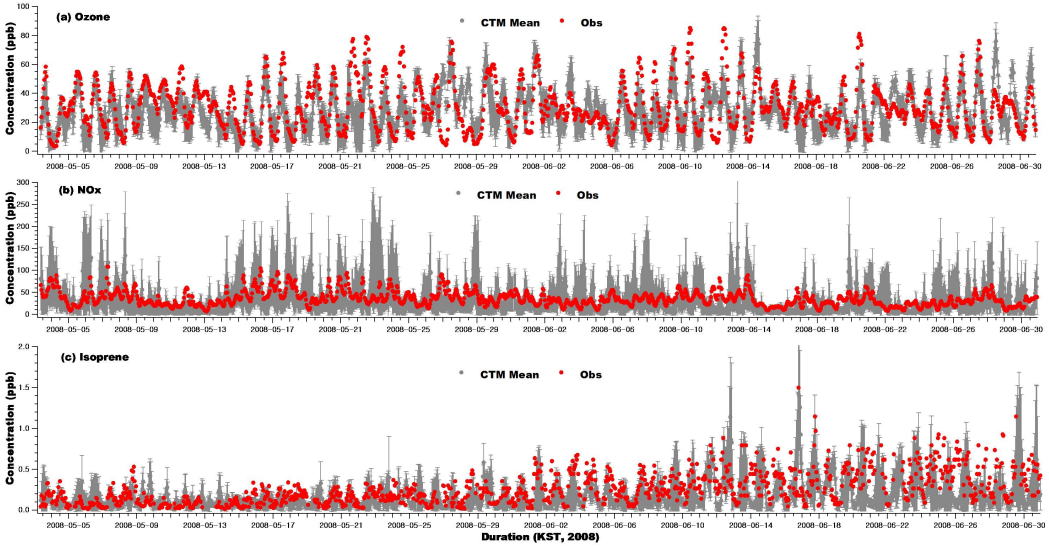

Fig. 6. Evaluation of CMAQ results for hourly O_3 concentrations. Note that "CTM Mean" represents the average of the CMAQ predicted O_3 concentrations from the three different BVOC scenarios, and "Obs" represents the average of measured O_3 concentrations at monitoring stations across the domain.

ACPD
13, 24925–24973, 2013

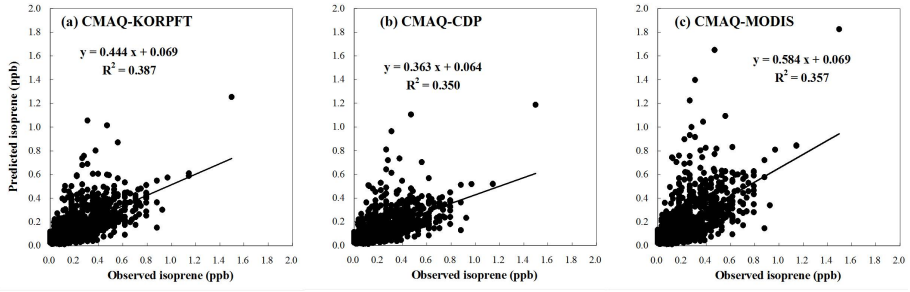

Fig. 7. Scatter plots of observed values versus CMAQ predicted isoprene for each BVOC emission scenario for the period of May–June 2008.

ACPD
13, 24925–24973, 2013

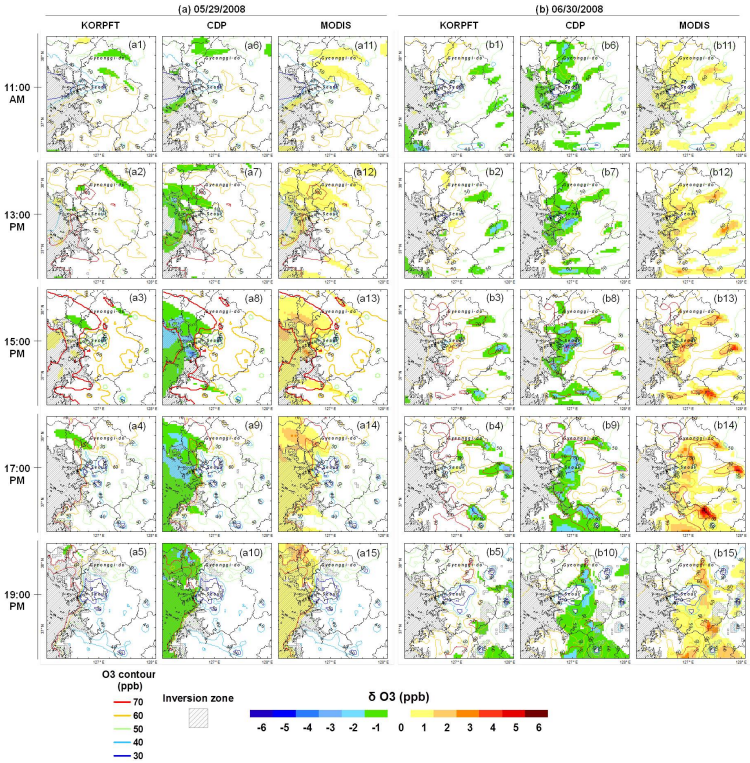

Fig. 8. Spatial distributions of CMAQ O_3 hourly deviations for each BVOC emission scenario and CMAQ mean O_3 hourly concentrations. The CMAQ mean O_3 hourly concentrations are the averaged values of CMAQ O_3 concentrations for the three PFT scenarios. These CMAQ O_3 concentrations were illustrates by the contour. The grey-hatched lines represent the temperature inversion zone.

ACPD
13, 24925–24973, 2013

Impacts of different plant functional types on ambient ozone predictions

H.-K. Kim et al.

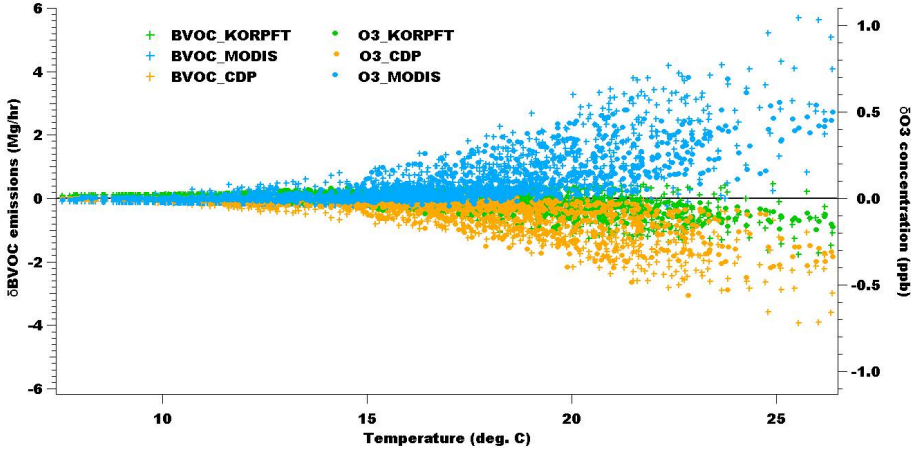

Fig. 9. Divergence of the predicted hourly BVOC emissions and O_3 concentrations with temperature change in the modeling domain. Every displayed value for δBVOC and δO_3 in this figure was derived from the hourly domain averaged values of the MEGAN BVOC emissions and CMAQ O_3 concentrations for the three PFT scenarios (e.g., KORPFT, CDP, and MODIS). The temperature on the horizontal axis in this figure represents averaged values of MM5-predicted ambient temperature.

ACPD
13, 24925–24973, 2013